Anisotropy of Radiation Damage in Electron-Bombarded Hexagonal Metals. II. A Model for Frenkel-Pair Formation in Single Crystals

F. Maury, P. Vajda, A. Lucasson, and P. Lucasson

Equipe de recherches du Centre National de la Recherche Scientifique, Laboratoire de Chimie Physique, F91405 Orsay, France
(Received 24 May 1973)

A "geometrical" model is presented for the hexagonal close-packed lattice proposing several principal mechanisms for the displacement of a knocked-on atom. Using the experimentally determined resistivity-change rates of a previous paper and matching families of cross sections computed with this model, we have calculated sets of thresholds energies for displacement in the directions [0001], [$10\bar{1}4$], [$10\bar{1}2$], [$10\bar{1}1$], and [$11\bar{2}0$] in cobalt, zinc, and cadmium. The correlation between the resistivity-change rates and the displacement cross sections allowed the determination of the Frenkel-pair resistivity per unit concentration in cobalt and zinc: $\rho_F^{Co} \approx 3\ \rho_0{}^\Omega{}_C$/at.%, $\rho_F^{Zn} = 3.5\ \rho_0{}^\Omega{}_C$/at.%; no definite conclusion for ρ_F^{Cd} could be made owing to the proximity of a recovery stage. Expressions for the energies needed to pass across one or several open "windows" in the hcp unit cell were derived, including the possibility of focusing collisions in the [$11\bar{2}0$] direction, and compared with the previously calculated threshold energies for displacement in various directions. This comparison permitted the tentative deduction of interatomic potentials of the Born–Mayer type giving as a possible choice: U^{Co}(eV) = $3300e^{-4.1r(Å)}$, U^{Zn}(eV) = $280e^{-2.5r(Å)}$, U^{Cd}(eV) = $300e^{-2.0r(Å)}$.

I. INTRODUCTION

It is by now a well-established phenomenon that atom displacements caused by collision with an energetic particle proceed preferentially in a few fundamental directions of the crystal lattice. In other words, the so-called threshold-energy surface contains distinct minima of generally 10–20° width around the principal low-index directions of a unit cell. This has been analyzed in detail for fcc[1] and bcc[2] lattices by the Brookhaven group, who simulated atomic collisions on a computer using a potential of the type

$$U(r) = A\ e^{-br} \quad , \tag{1}$$

with r as the interatomic distance. Using the results of the computer "experiments,"[1] Jan and Seeger[3] employed a threshold-energy surface which they gave an analytical form (harmonic) using three adjustable parameters for cubic crystals. A comparison of the experimental results and the cross section $\sigma(E)$ calculated with this analytical threshold-energy surface allowed a deduction of the three parameters, which were the displacement energy thresholds in the three main crystal directions ⟨100⟩, ⟨110⟩, and ⟨111⟩. This method was used to interpret the single-crystal results of nickel[4] and tantalum,[5] and also of hexagonal graphite[6] bombarded by electrons. We feel that this technique might be justified for crystals of a high symmetry such as the fcc system; but already in the case of the hexagonal close-packed (hcp) crystals, their relatively lower symmetry would induce us to choose more than three fundamental displacement mechanisms. In using Jan and Seeger's threshold-energy function, this would imply an increased number of parameters, thus complicating the analytical form of this function and making its application impractical. It seems, actually, that even for bcc crystals the Jan-Seeger method is not easily applicable: Jung and Schilling[5] had to cease in their efforts to fit their tantalum data with its help, and Lomer and Pepper[7] from the beginning used the computer results[2] instead of it for their iron interpretation.

In what follows, we propose a tentative model for the displacement events in an hcp lattice, proceeding from simple geometrical considerations concerning possible propulsion mechanisms of a knocked-on atom, without any *a priori* assumption for the form of the threshold-energy surface. Section II will present this "geometrical" model showing the various "easy" displacement directions. Section III will briefly treat the calculation method of the displacement cross section using the model described before, and in Sec. IV we shall, finally, compare the obtained families of displacement cross sections with experimental resistivity change rates measured for hcp, cobalt, zinc, and cadmium and presented in the preceding paper,[8] hereafter called I; this comparison shall offer us the right combination of threshold energies for the model in question. In Sec. V, we shall calculate the energies an atom needs to pass through various potential barriers in the corresponding directions and try to match an interatomic potential of the form (1) so as to reproduce the empirically obtained sets of thresholds.

II. DISPLACEMENT MECHANISMS IN AN hcp LATTICE

Figure 1 represents half the unit cell of an hcp crystal: We show one basal plane and the three
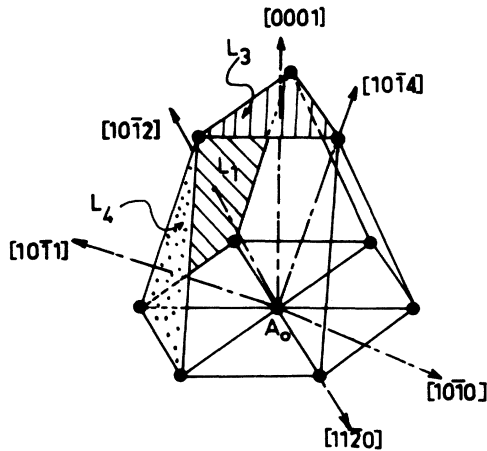
FIG. 1. Part of the hcp unit cell indicating several lenses and the corresponding propulsion directions of the atom A_0 across them.

atoms placed symmetrically half-way between this plane and the one in a distance c above it. We have indicated the principal directions which the central atom of the base plane will take when being knocked out of its lattice position: $[0001]$, $[10\bar{1}4]$, $[10\bar{1}2]$, $[10\bar{1}1]$, $[11\bar{2}0]$, and $[10\bar{1}0]$, which are perpendicular to the lattice planes (0001), $(30\bar{3}8)$, $(30\bar{3}4)$, $(30\bar{3}2)$, $(11\bar{2}0)$, and $(10\bar{1}0)$, respectively.

To illustrate better the various collision mechanisms, we present in Fig. 2 two projections of the ideal hcp lattice—very closely corresponding to the case of cobalt. In the upper part of the figure, we show the basal plane viewed along the c axis; in the lower part, we show a view perpendicular to it and cut along the $(11\bar{2}0)$ plane, i.e., under an angle of 30° with regard to the prismatic plane. The filled circles represent atoms in the plane of the paper; the open ones represent those in the plane immediately above or below it. Let us consider now the trajectories which the atom marked A_0 would take once it is pushed out of its lattice site, according to the principle of least effort. One can see that the atom is surrounded by different "lenses" of various shapes and sizes, which we shall describe here in some detail:

L_1: ideally a square lens of side length a, where a is the lattice constant of the basal plane. The atom A_{0_2}, which has been knocked into the direction $[10\bar{1}2]$ (cf. Fig. 1) and has passed through L_1 [parallel to the plane $(30\bar{3}4)$], will encounter the next atom A_1 after a distance $2a_1$ (a_1 is equal to the distance r_1 of the lens center to one of its atoms) and will push the latter through a very open lens L_2.

L_2: a wide rectangular lens parallel to the

(3038) plane with a center-to-atom distance r_2 and a relatively small lens "depth" a_2 such that the next chain atom A_2 is rather close. We shall call a collision of the type across L_2 into the direction $[10\bar{1}4]$ a "quasifocusing" collision, since it represents the beginning of a focusing chain (geometrically equivalent to the focusing chain in the $\langle 110 \rangle$ direction in an fcc lattice) which does not continue but drops its atom into another square lens of the type L_1.

The passage L_1-L_2-L_1, etc. is symmetrical: We can see, actually, that the atom A_0 can make first a quasifocusing collision (with B_1) and push the latter through a square lens L_1—it results in the sequence L_2-L_1-L_2, etc.

L_3: a triangular lens formed by the three atoms above or below the basal plane in a distance $\frac{1}{2}c$ (c is the lattice constant between two basal planes). The passage of A_0 across L_3 in the direction $[0001]$ will knock the next atom A_0' through an identical lens L_3 giving L_3-A_0'-L_3, etc.

L_4. another triangular lens, parallel to $(30\bar{3}2)$, which in the case of an ideal hcp lattice [where $c/a = (\frac{8}{3})^{1/2}$] equals L_3; for zinc and cadmium, with $(c/a)^2 > \frac{8}{3}$, this lens is bigger than L_3. By being pushed in the direction $[10\bar{1}1]$, the atom A_0 passes through a double lens L_4 before colliding with the next atom C_1—a situation analogous to that of an atom knocked into the direction $\langle 111 \rangle$ in an fcc
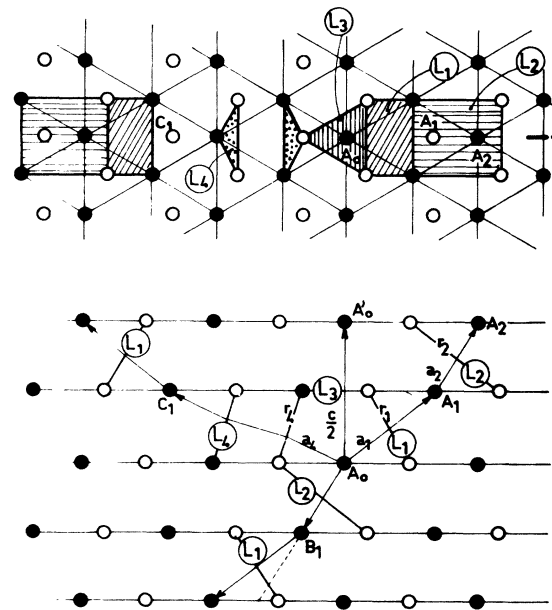
FIG. 2. Two views of the hcp lattice. Above: view along the c axis of the crystal; below: view perpendicular to the c axis, cut parallel to the $(11\bar{2}0)$ plane. Indicated are several of the lenses (cf. Fig. 1) and their dimensional characteristics.

TABLE I. Center-to-atom distances r_i and "depths" a_i of the various lenses in an hcp lattice (cf. Fig. 2).

L_i	r_i		a_i	
		ideal		ideal
L_1	$(\tfrac{1}{3}a^2 + \tfrac{1}{16}c^2)^{1/2}$	$\tfrac{1}{2}a\sqrt{2}$	$(\tfrac{1}{3}a^2 + \tfrac{1}{16}c^2)^{1/2}$	$\tfrac{1}{2}a\sqrt{2}$
L_2	$(\tfrac{7}{12}a^2 + \tfrac{1}{16}c^2)^{1/2}$	$\tfrac{1}{2}a\sqrt{3}$	$(\tfrac{1}{12}a^2 + \tfrac{1}{16}c^2)^{1/2}$	$\tfrac{1}{2}a$
L_3		$\tfrac{1}{3}a\sqrt{3}$	$\tfrac{1}{2}c$	$a\left(\tfrac{2}{3}\right)^{1/2}$
L_4	$\dfrac{\tfrac{1}{3}a^2 + \tfrac{1}{4}c^2}{(\tfrac{1}{3}a^2 + c^2)^{1/2}}$	$\tfrac{1}{3}a\sqrt{3}$	$\dfrac{a\sqrt{3}}{3}\left[\left(1+\dfrac{1+x}{1+4x}\right)^2 + x\left(1-2\dfrac{1+x}{1+4x}\right)^2\right]^{1/2}$,	$a\left(\tfrac{2}{3}\right)^{1/2}$

with $x = \tfrac{3}{4}(c/a)^2$

| L_5 | $r'_5 = \tfrac{1}{2}a\sqrt{3}$ | | $\tfrac{1}{2}a$ | |
| | $r''_5 = (\tfrac{1}{12}a^2 + \tfrac{1}{4}c^2)^{1/2}$ | $\tfrac{1}{2}a\sqrt{3}$ | | |

lattice. The further track, however, is different from the fcc trajectory: C_1 is pushed across an L_1-type lens and now follows the sequence L_1-L_2-L_1, etc.

L_5: is not a lens in the exact sense used here. It is the classical focusing collision chain in all the directions of the type $[11\bar{2}0]$ in the basal plane, with an interatomic collision distance of a. The correction due to the interaction with the next-nearest atoms from the center between two chain atoms will be considered.

In Table I we have collected the necessary information concerning the sizes and "depths" of the

above-mentioned lenses for a general hexagonal close-packed lattice. The expressions are thus directly applicable for the zinc and cadmium cases as well: In fact, due to the larger c/a ratio of these metals, the lenses L_1, L_2, and especially L_4 become wider than in the ideal hcp crystal. The much simpler formulas for the ideal case of cobalt are also presented.

III. COMPUTATIONAL METHOD

Our task is the calculation of the displacement cross section, which is function of the bombarding electron energy E, such that

$$\sigma(E) = \int_{\alpha_2} \int_{\varphi_2} d\Omega_2 \left(\int_{\alpha_1} \int_{\varphi_1} [P(\alpha_1) d\alpha_1 d\varphi_1 / 2\pi] \frac{d\sigma(T,E)}{d\Omega_2} p(T, \alpha_2, \varphi_2) \right). \quad (2)$$

The relationship between the angles involved is illustrated in Fig. 3: α_1 and α_2 are counted from the direction of the incident electrons, φ_1 and φ_2 are perpendicular to it. The direction of the scattered electron is defined by the angles (α_1, φ_1), that of the recoil atom by (α_2, φ_2). $P(\alpha_1)$ is the angular dispersion function of the electrons in the specimen (cf. the discussion in I, Sec. IV), which is supposed to be of Gaussian shape and normalized such that $\int_0^\pi P(\alpha)d\alpha = 1$. The angle between the knocking-electron direction and that of the knocked-on recoil atom is given by

$$\cos\theta = \sin\alpha_1 \sin\alpha_2 \cos(\varphi_2 - \varphi_1) + \cos\alpha_1 \cos\alpha_2. \quad (3)$$

The energy T transmitted to the atom by the incident electron is a function of θ

$$T = T_m \cos^2\theta, \quad (4)$$

where T_m is the maximum energy transferable in

a head-on collision: $T_m(\text{eV}) = (560.8/A)\epsilon(\epsilon + 2)$, with $\epsilon = E/m_0 c^2$ and the usual meaning of the notations. For the differential cross section $d\sigma/d\Omega_2(T, E)$, we employ the approximate formula by McKinley and Feshbach,[9] and $p(T, \alpha_2, \varphi_2)$ is the step probability of an atom having received the energy T in the direction (α_2, φ_2) to be displaced:

$$p(T, \alpha_2, \varphi_2) = 0 \text{ for } T(\theta) < T_d(\alpha_2, \varphi_2),$$

$$= 1 \text{ for } T(\theta) \geq T_d(\alpha_2, \varphi_2). \quad (5)$$

In expression (5) the main difficulty of the problem emerges: in order to be able to calculate the cross section (2), we have to know $T_d(\alpha_2, \varphi_2)$. In fact, what we shall do is to invert the procedure and use sets of T_d's as parameters, subdividing the space $\Omega_2 = (\alpha_2, \varphi_2)$ into a number of distinct "windows" corresponding to the "lenses" presented in Sec. II, where the various T_d's will assume a constant and
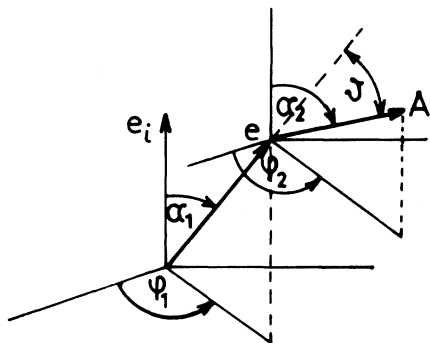
FIG. 3. Angles relating the directions of the knocking electron and of the recoil atom to the direction of the incident electrons.

relatively low value. In between the windows, the space is supposed to be nontransparent for the recoil atoms, i.e., we shall assign it to a T_d which is not attainable by the maximum energies transferred in our experiment. An additional parameter is the size of the various windows, for which we shall be guided by the geometrical considerations of Sec. II and by the results of the Brookhaven group[1,2] concerning the region of constant minimum threshold around a low-index crystallographic direction. The obtained families of cross sections will then be compared with the experimental damage-rate curves with the aim of choosing the right set of T_d's. It may seem that the picture of a window with a constant T_d surrounded by a space of much larger T_d is not justified. In fact, such an image of something like a potential well is what follows from the computer simulations. It will be more or less correct if the respective interatomic potentials are more or less steep. As a first approximation, we have defined the windows corresponding to the selected orientations by a solid angle of rotation of 10° around the focusing direction [11$\bar{2}$0] and of 20° around the other directions. The calculations showed, however, that it was not sufficient to consider the first collision only, since the atom would not stay permanently displaced after the passage of only one lens system. Taking into account more than one passage changes the symmetry properties of the problem and leads to a modification of the shape of the windows. The finally adopted threshold-energy surface is shown in a stereographic projection in the upper part of Fig. 4 viewed along the c axis of the crystal. We note that directly adjoining the central lens (0001) there are three windows corresponding to the quasifocusing direction $\langle 10\bar{1}4 \rangle$ with the threshold energy T_2. The opening angle of these windows is nonsymmetrical to facilitate the subsequent passage of the recoil atom through L_1. The window L_1 had under-

gone an analogous treatment. For the same reason, the window L_4 is divided into a region with a threshold T_4 and another region with a threshold T_4' which can be larger or smaller than T_4, thus allowing the passage through both triangular lenses L_4 only for the right combination of (α_2, φ_2). The lower part of Fig. 4 represents a cut parallel to the (11$\bar{2}$0) plane and delineates the opening angles of the various windows.

A particular problem to mention is the multiple-defect creation. In order to take into account the multiplication of defects, we have to introduce the coefficient $\nu = T/2T_d$ from the moment when $T > 2T_d$. The difficulty arising here stems from the fact that—due to the angular dispersion of the electrons—one might in a certain direction still be in the region $T < 2T_d$, but in another (easier) direction, with a smaller threshold T_d, to attain values where the cascade formation might become effective. In any case, the correction for this effect never sur-
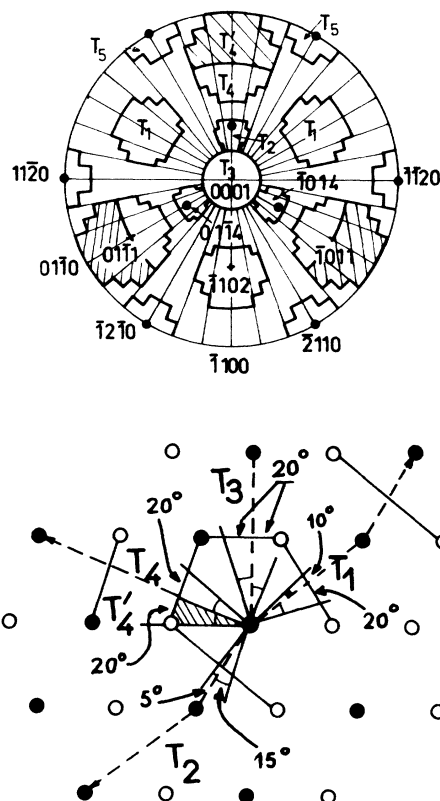
FIG. 4. Above: stereographic projection of the threshold-energy surface viewed along the c axis of the crystal indicating the various open windows having the respective thresholds T_i. The shape of the windows corresponds to the form they have been given for the computation. Below: cut parallel to the (11$\bar{2}$0) plane indicating the opening angles of the windows.

passes ~ 15% at the highest energy (1. 7 MeV) used. But, in principle, the problem remains open and is a limitation for any simplified model.

As concerns the incident beam dispersion due to the passage through various windows and the sample itself, we have adopted a mean thickness of the specimen for which the Gaussian $P(\alpha_1)$ was applied in the form (7) of L No corrections have been made for energy loss and increase of path length of the incident electrons in the specimen, or for an eventually nonuniform defect distribution across its thickness. These corrections would only be of importance near E_d, where the relative errors are particularly large and the data are less reliable, while we are attempting to reproduce the shape and the relative positions of the damage-rate curves in the whole energy range studied—certainly a safer way of tackling the problem.

The integration was performed on an IBM-375 computer of the CIRCE Computational Center at Orsay; details of the program are given in Ref. 10.

IV. COMPARISON WITH EXPERIMENT

In this section, we present the calculations made for cobalt, zinc, and cadmium and compare them with the results obtained experimentally and published in I. The influence of a variation of different parameters such as the values of threshold energies will be shown in detail for the case of cobalt. Only final results will be presented for zinc and cadmium.

A. Cobalt

Figure 5 shows the results acquired for cobalt: Figure 5(a) has been taken from Paper I and reproduces the experimental data, Fig. 5(b) represents our closest agreement achieved computationally. The agreement is not really perfect, but in view of the limitations of our model it is satisfactory. In fact, the main features such as the shape of the curves and their relative positions with regard to each other [always maximum for (0001) and minimum for (11$\bar{2}$0)], with the three other orientations hardly distinguishable) are corroborated, the only shortcoming is the slightly too high data of the (11$\bar{2}$0) specimen. In the framed case, we indicate the mean thickness $\bar{x}$ used in the calculations and the five threshold energies of the various windows in the respective directions employed as parameters for the given set of curves.

We propose for the main threshold-energy regions in cobalt the following values:

[0001]: $T_3 = 40 \pm 3$ eV,

[10$\bar{1}$4]: $T_2 = 23 \pm 2$ eV,

[10$\bar{1}$2]: $T_1 = 22 \pm 1$ eV,

[10$\bar{1}$1]: $T_4 = 40 \pm 5$ eV

(upper-half of L_4 in Fig. 4)

[11$\bar{2}$0]: $T_5 = 27 \pm 2$ eV;

for all intermediate directions: $T_d > 150$ eV.

In order to demonstrate how sensitive our procedure was to a variation of one or several thresholds, we have chosen among roughly two hundred families of cross sections with various sets of parameters; the effect is shown in Figs. 5(c)–5(f). We might also mention that a change of the mean thickness $\bar{x}$ to 30 μ did not influence the results much, while a reduction to 12 μ introduced nonobserved structures; we are thus retaining 20 μ as a reasonable and experimentally justified choice. The fact that the (0001) crystal exhibits highest damage rates over the whole energy range implies minimum threshold energies in both neighboring lenses L_2 and L_1, i. e., in the directions [10$\bar{1}$4] and [10$\bar{1}$2]. An increase of one of these thresholds immediately lowers the (0001) curve; namely, at the low-energy end when diminishing T_2, and at higher energies when lowering T_1. A reduction of the threshold for the [0001] direction increases the difference between (30$\bar{3}$8) and (30$\bar{3}$4) on the one hand and (10$\bar{1}$0) on the other. A diminution of the [11$\bar{2}$0] threshold increases exaggeratedly the results of the (11$\bar{2}$0) crystal at intermediate energies and those of the (10$\bar{1}$0) sample at lower ones.

Howe[11] has irradiated monocrystalline cobalt in an electron microscope and observed the following thresholds:

[0001]: 33 ± 1 eV,

[10$\bar{1}$0]: 30 ± 1 eV,

[11$\bar{2}$0]: 23 ± 0. 5 eV.

There is an apparent disagreement with our findings, but one has to remember that the measured threshold energy of 33 eV for the [0001] orientation can either mean a $T_d = 33$ eV in this direction or—considering that 33 eV = 22 eV/cos²35°—a $T_d \approx 22$ eV in the direction [10$\bar{1}$4]. In the same way, the [10$\bar{1}$0] threshold of 30 eV can be due to a real threshold energy of ~ 23 eV in the [11$\bar{2}$0] or in the [10$\bar{1}$2] direction. All this is in quite satisfactory agreement with our analysis. The only difficulty is the somewhat higher value of 27 eV which we obtain for the [11$\bar{2}$0] orientation. We have no direct explanation for this; possibly, the fact that our specimens had a rather high impurity concentration, which could interfere with the propagation of focusing chains, might be at the origin of this discrepancy.

Another comparison is given by the results on polycrystalline cobalt, [12] where a fit of the experimental data had been achieved using a three-step probability function with steps at 22. 5, 28, and 35 eV, respectively. A juxtaposition with our single-crystal results leads to the attribution of the first step to displacements in [10$\bar{1}$4] and [10$\bar{1}$2] directions, the second step would be due to a focusing
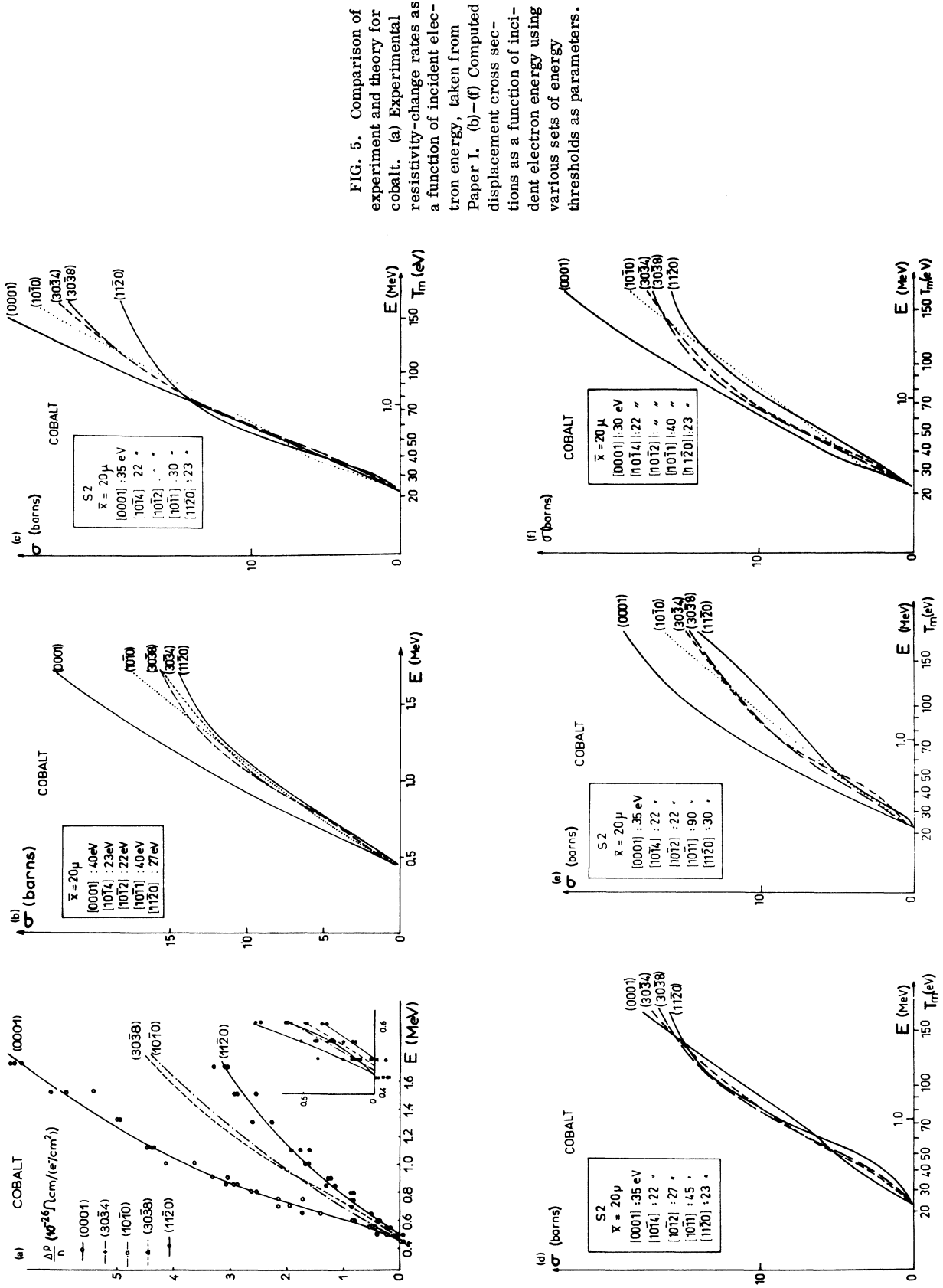
FIG. 5. Comparison of experiment and theory for cobalt. (a) Experimental resistivity-change rates as a function of incident electron energy, taken from Paper I. (b)–(f) Computed displacement cross sections as a function of incident electron energy using various sets of energy thresholds as parameters.

(a) COBALT

$\frac{\Delta\rho}{n}$ (10⁻²⁶ Ωcm/(e/cm²))

(0001)
(30̄3̄4)
(10̄1̄0)
(30̄3̄8)
(112̄0)

(b) COBALT

σ (barns)

x̄ = 20μ

[0001] : 40 eV
[10̄1̄4] : 23 eV
[10̄1̄2] : 22 eV
[10̄1̄1] : 40 eV
[112̄0] : 27 eV

(0001)
(10̄1̄0)
(30̄3̄8)
(30̄3̄4)
(112̄0)

E (MeV)

(c) COBALT

σ (barns)

S2
x̄ = 20μ

[0001] : 35 eV
[10̄1̄4] : 22 "
[10̄1̄2] : 22 "
[10̄1̄1] : 30 "
[112̄0] : 23 "

(0001)
(10̄1̄0)
(30̄3̄4)
(30̄3̄8)
(112̄0)

E (MeV) Tm (eV)

(d) COBALT

σ (barns)

S2
x̄ = 20μ

[0001] : 35 eV
[10̄1̄4] : 22 "
[10̄1̄2] : 27 "
[10̄1̄1] : 45 "
[112̄0] : 23 "

(0001)
(30̄3̄4)
(30̄3̄8)
(112̄0)

E (MeV) Tm (eV)

(e) COBALT

σ (barns)

S2
x̄ = 20μ

[0001] : 35 eV
[10̄1̄4] : 22 "
[10̄1̄2] : 22 "
[10̄1̄1] : 90 "
[112̄0] : 30 "

(0001)
(10̄1̄0)
(30̄3̄4)
(30̄3̄8)
(112̄0)

E (MeV) Tm (eV)

(f) COBALT

σ (barns)

x̄ = 20μ

[0001] : 30 eV
[10̄1̄4] : 22 "
[10̄1̄2] : 22 "
[10̄1̄1] : 40 "
[112̄0] : 23 "

(0001)
(10̄1̄0)
(30̄3̄4)
(30̄3̄8)
(112̄0)

E (MeV) Tm (eV)

mechanism in the [11$\bar{2}$0] direction, and the third step might be correlated with [0001] and [10$\bar{1}$1] displacements.

Finally, to obtain direct comparison between Figs. 5(a) and 5(b), we have to convert the resistivity-change rates to cross sections through the introduction of ρ_F, the resistivity of a unit concentration of Frenkel pairs (cf., also, the discussion in I, Sec. IV):

$$\Delta\rho/n = \sigma(E)\rho_F \ . \tag{6}$$

The corresponding value for ρ_F lies, in the case of cobalt, between 20 and 50 μohm cm/at.% for the various orientations, in average ~30 μohm cm/at.% While the empirically derived relationship[13] gives $\rho_F \approx \rho_0 °c$ within a factor of 2, it was shown that for polycrystalline cobalt[12] one had already to assume at least $\rho_F = 2\rho_0$ to get agreement with the experimental data. In our experiment, we find $\rho_F \gtrsim 3\rho_0$, which gives weight to the polycrystal results. This is just another proof for the need of experiments with single crystals and of a thorough analysis of the data obtained in order to get information on the basic characteristics of point defects.

B. Zinc

In Fig. 6, we present the experimental results [Fig. 6(a)] taken from Paper I and the best fit obtained by computation [Fig. 6(b)]. The agreement is very close and we rather confidently propose as the optimum set of thresholds:
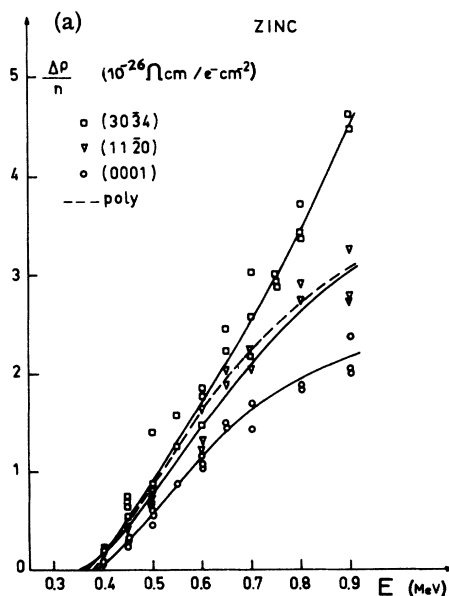
[0001]: $T_3 = 19^{+2}_{-1}$eV ,

[10$\bar{1}$4]: $T_2 = 25 \pm 2$eV ,

[10$\bar{1}$2]: $T_1 = 30 \pm 5$eV ,

[10$\bar{1}$1]: $T'_4 = 20 \pm 2$eV ,

(lower-half of L_4 in Fig. 4),

[11$\bar{2}$0]: $T_5 = 14^{+2}_{-1}$eV ,

for all intermediate directions: $T_d > 55$ eV.

As in the case of cobalt, it is interesting to note that the analysis of the experiments on polycrystalline zinc[14] had yielded a double-step probability function, with the first step at 13.5 eV and the second at 18 eV. The analysis of the single-crystal data allows us now to assign the first step to focused collision chains and the second to displacements in the directions [0001] and [10$\bar{1}$1].

The correlation of Figs. 6(a) and 6(b) leads to a Frenkel-pair resistivity of $\rho_F = 20 \pm 3$ μohm cm/at.%, which means $\rho_F \approx 3.5\rho_0$ °c, quite comparable to the cobalt results.

C. Cadmium

Figure 7 shows the agreement between the experiment [Fig. 7(a) is the size-effect corrected plot of the data taken from I] and the best fit achieved with a given set of thresholds [Fig. 7(b)]. In fact, it turned out that it was sufficient to adjust only two threshold parameters keeping the others above a certain value. We propose the following threshold energies:
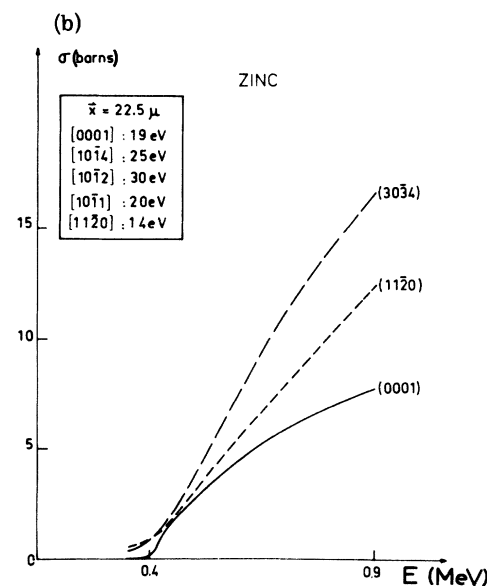
FIG 6. (a) Experimental resistivity-change rates as a function of incident electron energy for zinc, taken from Paper I. (b) Computed displacement cross sections with the best-fit set of energy thresholds.

[0001]: $T_3 \gtrsim 40$ eV ,

[10$\bar{1}$4]: $T_2 \gtrsim 35$ eV ,

[10$\bar{1}$2]: $T_1 \gtrsim 35$ eV ,

[10$\bar{1}$1]: $T_4 = 19 \pm 1$ eV

(upper half of L_4 in Fig. 4) ,

[11$\bar{2}$0]: $T_5 = 21^{+2}_{-1}$ eV ,

for all intermediate directions: $T_d > 40$ eV.

The data obtained for polycrystalline cadmium[15] did not permit an unambiguous determination of a probability function: It was only clear that at least two steps were needed and that the first step corresponded to a threshold value of $T_d = 19-20$ eV. The results of this paper allow an assignment of this threshold energy to displacements in the [10$\bar{1}$1] and/or [11$\bar{2}$0] directions, the displacements in other principal orientations being more "difficult."

The derived Frenkel-pair resistivity ρ_F gives a value of $\rho_F = 5 \pm 1$ μohm cm/at.%, which corresponds to $\rho_F \lesssim \rho_0$ °C, in contrast to the findings for cobalt and zinc. One must not forget, however, the main experimental difficulty discussed *in extenso* in Paper I: i.e., the rather low recovery temperature of Frenkel pairs in cadmium. Actually, it is not at all improbable that only a fraction of the created defects remain stable near the irradiation temperature, thus giving a reduced apparent ρ_F. This effect is also corroborated by the very low measured-resistivity-change rates in cadmium.

V. DEDUCTION OF INTERATOMIC POTENTIALS

As a next step, we shall try to calculate what minimum energy has to be imparted to the atom A_0 (see Figs. 1 and 2) in a head-on collision when we want it to pass through a certain lens (or several of them) and either to come to rest itself as a stable interstitial or in one way or another to provoke the formation of a Frenkel pair. The value thus obtained will correspond to the respective threshold energy for displacement of the atom A_0 in the direction in question, provided the interatomic potential has been chosen correctly. We shall employ here the inverse procedure, namely, derive expressions for the threshold energies where the potential shows up as a parameter to be adjusted so as to render agreement with the experimental findings. For this, we shall use a Born-Mayer-type interatomic potential of the form (1).

For each lens passage, we have to distinguish between two cases: The first where the moving atom loses its total kinetic energy and becomes interstitial immediately after passage through the lens, and the second where the atom has retained enough energy to push the atom in front out of its lattice site and replace it there. We shall call these two cases the "last sequence" and the "penultimate sequence," respectively. In this sense, the latter term will designate all the passages not resulting in the formation of an interstitial. The actual number of sequences to calculate will depend on the stability of the resulting
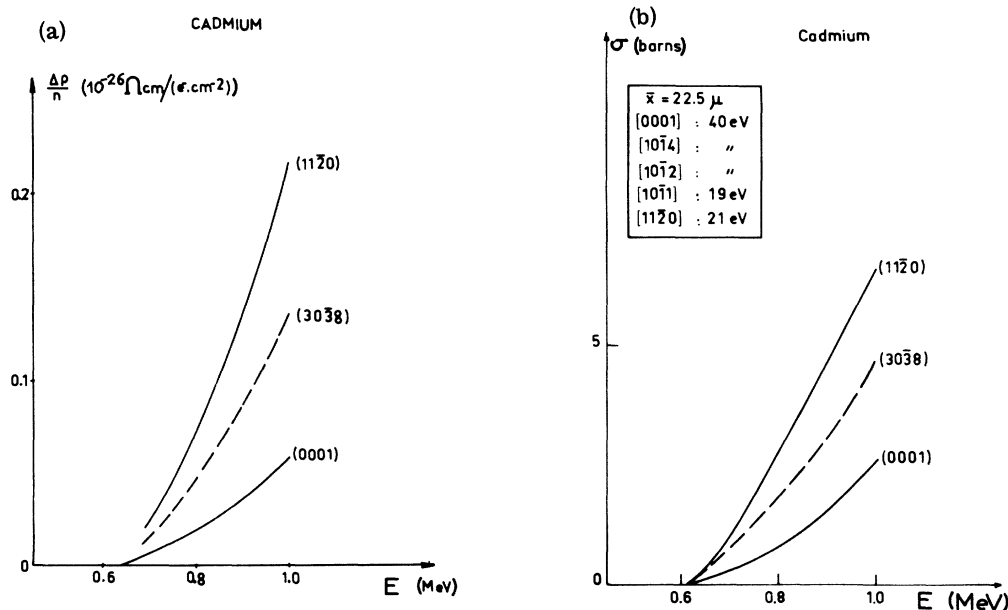
FIG. 7. (a) Size-effect corrected experimental resistivity-change rates as a function of incident electron energy for cadmium, taken from I. (b) Computed displacement cross sections with the best-fit set of energy thresholds.
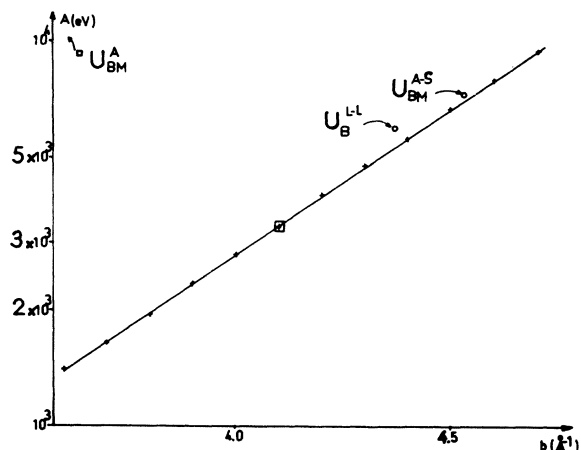
FIG. 8. Relation between the Born-Mayer-potential constants A and b for cobalt in the range applicable to our model. Indicated are the constants for the potentials U_{BM}^A, U_{BM}^{A-S}, and U_B^{L-L} derived from the Refs. 16–18, and our proposed choice.

Frenkel pair and is subject to discussion. The principle of the calculations being the same for all lenses, except for the special problem of a focused collision chain, we shall give an example of it for the two cases in the Appendix.

A. Cobalt

The close values obtained for T_1 (square lens in the [$10\bar{1}2$] direction) and for T_2 (quasifocusing in the [$10\bar{1}4$] direction) imply a sequence choice of L_2-L_1-L_2 or L_2-L_1-L_2-L_1 on the one hand, and L_1-L_2-L_1 on the other. The uncertainty of these thresholds does not permit the evaluation of each of the potential constants A and b but only of the pair of them, with a relatively wide variation range. Figure 8 shows the relation between A and b, which can be expressed by $A/eV = 2.3\,e^{4.77b/\text{Å}-1}$.

Table II gives the threshold energies for displacement in the investigated directions for three couples of the potential constants (A, b) taken from Fig. 8. A separation by three or four lenses of the type L_1 and L_2 means that the interstitial is four to five interatomic distances away from its vacancy. The computer simulations[1,2] have shown that such Frenkel pairs can be stable. The corresponding spontaneous recombination volume of ~100 atomic volumes also gives the right order of magnitude. Furthermore, we note the smaller threshold in the [$10\bar{1}4$] direction when passing through a four-lens system L_2-L_1-L_2-L_1 as compared to a passage through only three lenses of this type, using the steepest potential. The explanation lies in the fact that, in our approximation and with this potential, the knocked-on atom will not stop at the lens L_2 but, possessing enough kinetic energy, will move on and become an interstitial only after hav-

ing pushed the next atom. This is not the case with the two softer potentials. The relatively high threshold in the [0001] direction allows only for one passage across L_3; a stability of such a Frenkel pair is not impossible, since it was shown[1,2] that the spontaneous-recombination distances were small when the neighbor atoms of the interstitial were pushed not towards the vacancy but in another direction, which is the case here.

A more serious difficulty is the passage in the [$10\bar{1}1$] direction. For the otherwise favorable combination $A = 8000$ eV, $b = 4.60$ Å^{-1}, we obtain, here, just one passage across the double lens L_4. A stable interstitial at such a small distance in this direction would be in contradiction with the computer results[1] for the fcc structure. We must remember, however, that the matter looks different in an hcp lattice. While in an fcc crystal an atom which has passed through two triangular lenses in the corresponding [111] direction pushes its counterpart into a tightly squeezed position between two identical lenses, in an hcp structure, such an atom faces the much easier task of projecting its counterpart across a relatively wide square lens of the type L_1 with a lower potential barrier. Therefore, this configuration might well be stable. Another valid solution to the problem could be the breaking up of the single-step probability function in the [0001] direction

$$p_{[0001]} = 0 \text{ for } T < 40 \text{ eV },$$

$$= 1 \text{ for } T \geq 40 \text{ eV },$$

into a double-step one of the form

$$p_{[0001]} = 0 \text{ for } T < 33 \text{ eV },$$

$$= 0.5 \text{ for } 33 \leq T < 55 \text{ eV },$$

$$= 1 \quad \text{ for } T \geq 55 \text{ eV }.$$

The calculations performed with this latter function have in fact shown that the best fit of Fig. 5(b) does not change. Physically, this would mean that

TABLE II. Threshold energies for displacement in different directions and for different lens combinations in a cobalt crystal calculated with various Born-Mayer constants (A, b).

Displacement directions		A/eV	Threshold energies/eV		
		$b/\text{Å}^{-1}$	8000	2800	1400
			4.60	4.00	3.60
[0001]	L_3		39.1	31.8	27.6
	$L_3 - L_3$		68.2	55.8	48.9
[$10\bar{1}4$]	$L_2 - L_1 - L_2$		24.5	21.3	19.8
	$L_2 - L_1 - L_2 - L_1$		23.4	23.7	24.1
[$10\bar{1}2$]	$L_1 - L_2 - L_1$		22.1	22.1	22.1
[$10\bar{1}1$]	L_4		39.4	32.0	27.8
	$L_4 - L_1$		45.0	38.1	34.4
[$11\bar{2}0$]	9 collisions		26.0	26.0	27.1
	10 collisions		27.6	28.0	29.5

TABLE III. Threshold energies for displacement in different directions of a zinc crystal for different lens combinations and with various Born—Mayer constants (A, b).

		Threshold energies/eV		
	A/eV	550	280	155
Displacement directions	$b/Å^{-1}$	3.0	2.5	2.0
[0001] $\quad L_3$		18.6	18.5	18.5
[10ī4] $\begin{cases} L_2-L_1-L_2-L_1 \\ L_2-L_1-L_2-L_1-L_2 \end{cases}$		14.9 18.7	20.0 24.4	29.0 35.1
[10ī2] $\begin{cases} L_1-L_2-L_1 \\ L_1-L_2-L_1-L_2 \\ L_1-L_2-L_1-L_2-L_1 \end{cases}$		13.3 17.0 21.1	17.2 21.5 28.3	23.8 29.7 41.3
[10ī1] $\begin{cases} L_4 \\ L_4-L_1 \end{cases}$		13.9 18.4	14.2 20.9	14.3 25.1
[11ī0] $\begin{cases} \text{4 collisions} \\ \text{5 collisions} \end{cases}$		9.4 11.0	11.6 14.3	16.5 21.6

the threshold for passing through one lens L_3 is 33 eV, but the atom has, in this case, only the probability $\frac{1}{2}$ to form a stable interstitial unless it moves across a second lens L_3, in which case it needs in total 55 eV. With this argument, a good choice for the potential constants would be $A = 3300$ eV, $b = 4.10 Å^{-1}$.

Abrahamson[16] has proposed for each element a best Born-Mayer approximation to the statistical Thomas-Fermi-Dirac potential for interatomic distances of 1–2 Å. His values for cobalt $(A = 12600$ eV, $b = 3.57 Å^{-1})$ furnish far too high energies. However, Andersen and Sigmund's[17] semi-empirical relationship $A = (52$ eV$) Z^{3/2}$, $b = $ const $= 4.56 Å^{-1}$, seems to be not too bad a choice for cobalt: giving $A = 7300$ eV, $b = 4.56 Å^{-1}$, it is well placed on our (A, b) curve of Fig. 8. Lucasson and Lucasson[18] have performed a similar calculation for fcc metals and obtained potential constants for nickel, copper, silver, and gold using a Bohr potential of the type $U(r) = (Z^2 e^2/r) e^{-br}$. Matching this potential to a Born-Mayer potential of the type (1) and choosing its pre-exponential factor and the constant in the exponent so as to obtain the threshold energy in one of the easy displacement directions yields for cobalt: $A = 5960$ eV, $b = 4.37 Å^{-1}$, also in good agreement with our own findings.

B. Zinc

Again, as in the case of cobalt, we propose pairs of potential constants (A, b) as possible choices: Table III gives the calculated thresholds for three combinations (A, b) which have been adjusted so as to yield the right threshold energy T_3 in the direction [0001] after one passage across the triangular lens L_3. The corresponding potentials have been designed in Fig. 9. One can see that softening of the potential by decreasing the constant b renders more favorable the passage across triangular

lenses than that across rectangular ones. If one assumes that the Frenkel-pair stability is the same in the cases of cobalt and of zinc {three passages necessary through the rectangular lens (30$\bar{3}$8) in the direction [10$\bar{1}$4]}, one obtains $b = 2.0 Å^{-1}$; if, however, one admits a lesser stability for zinc, i.e., five passages across (30$\bar{3}$8) and (30$\bar{3}$4) needed for the creation of a stable interstitial, the choice would be rather $b = 2.5 Å^{-1}$.

As a final remark, we wish to add that for highly anisotropic crystals such as zinc one may wonder about the justification to employ a spherically symmetric potential like the one used. The results presented should thus be taken as an indication only.

A comparison with the existing estimates by Abrahamson[16] $(U/eV = 14\,700 e^{-3.56r/Å})$, by Andersen and Sigmund[17] $(U/eV = 8500 e^{-4.56r/Å})$, and by matching to a Bohr potential[18] $(U/eV = 6640 e^{-3.82r/Å})$ shows them to be far off our findings. This is not too surprising, since Abrahamson does not take into account any crystallographic properties of the substance considered but only its atomic characteristics, while the two latter methods construct their empirical potentials basing on experimental data for copper and other cubic metals; this might also explain the good agreement with cobalt, which, being an almost ideal hcp crystal, comes quite close to fcc copper.

C. Cadmium

Cadmium being crystallographically very similar to zinc, the same reservations should be made
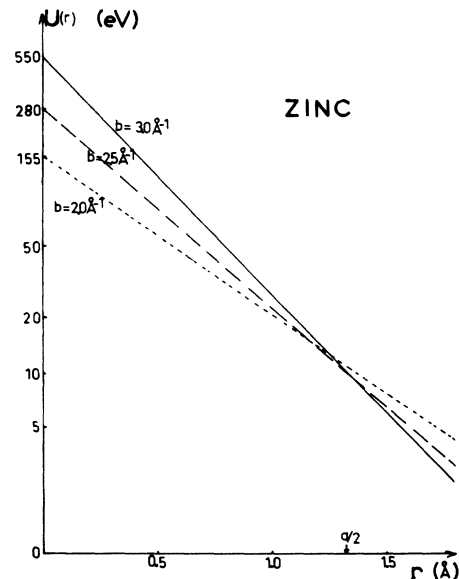
FIG. 9. Various possible Born—Mayer-type interatomic potentials for zinc.

TABLE IV. Displacement thresholds for cadmium in different directions using the potential $U/eV = 300\,e^{-2.0r/Å}$.

Displacement directions		Threshold energies/eV
[0001]	$L_3 - L_3$	52
[10$\bar{1}$4]	$L_2 - L_1 - L_2 - L_1$	34
[10$\bar{1}$2]	$L_1 - L_2 - L_1 - L_2$	36
[10$\bar{1}$1]	L_4	20
[11$\bar{2}$0]	{ 4 collisions	20
	{ 5 collisions	25

when determining an interatomic potential. Moreover, as we have seen in Sec. IV, the matching of the computed cross sections to the experimental damage-rate curves is not very sensitive to the choice of T_1, T_2, and T_3 as long as they are large enough. As an example, we demonstrate in Table IV the thresholds calculated with the potential $U/eV = 300\,e^{-2.0r/Å}$.

One notes that the interstitials produced by the electrons of $\lesssim$ 1-MeV energy (corresponding to $T \lesssim 30$ eV) are separated by only three to four interatomic distances from their vacancy and that they are close to the original basal plane. This might explain the very low recovery temperature and the simple annealing mechanisms of these pairs, as was reported in I (one simple peak at ~5 °K). Increasing the incident electron energy to 1.7 MeV renders possible other defect-production mechanisms and, indeed, the annealing spectrum becomes more complicated revealing a substage at 6–9 °K (cf. Table III of Paper I). This interpretation does conform with the recovery processes invoked by Coltman et al.,[19] who explain the low-temperature recovery of their neutron-bombarded cadmium specimens as due to close Frenkel pairs situated either in the same basal plane or perpendicular to it.

The potentials of Ref. 16–18 are equally far off as in the case of zinc.

VI. CONCLUSION

A "geometrical" model is presented for the hcp lattice putting forward several principal mechanisms for the displacement of a knocked-on atom. Using the experimentally obtained resistivity-change rates as a function of the incident electron energy published in the Paper I and matching families of cross sections computed with the above model we have determined sets of threshold energies for displacement in cobalt, zinc, and cadmium given in Table V.

The correlation between the resistivity-change rates and the displacement cross sections allowed the determination of the Frenkel-pair resistivity per unit concentration in cobalt and zinc:

$\rho_0^{Co}{}_C \approx 30\,\mu\Omega\,cm/at.\%$,

$\rho_F^{Zn} \approx 3.5\,\rho_0^{Zn}{}_C = 20 \pm 3\,\mu\Omega\,cm/at.\%$;

no definite conclusion for ρ_F^{Cd} can be made owing to the proximity of a recovery stage.

We have derived expressions for the energies needed to pass across one or several open "windows" in the hcp unit cell, including the possibilities of focusing collisions in the [11$\bar{2}$0] direction, and compared them with the previously calculated threshold energies for displacement in various directions. This comparison enabled us to deduce tentatively interatomic potentials of the Born-Mayer type giving as a possible choice:

$U^{Co}/eV = 3300e^{-4.1r/Å}$,

$U^{Zn}/eV = 280e^{-2.5r/Å}$,

$U^{Cd}/eV = 300e^{-2.0r/Å}$.

APPENDIX: CALCULATION OF THRESHOLD ENERGIES

A. Last Sequence

In order to arrive at the saddle point O of Fig. 10, which is the center of a lens consisting of n atoms $B_1, \ldots, B_n$, the atom A_0 has to possess at least the energy

$$U_1 = nU(OB_i) = nU(r_i) ,\qquad (A1)$$

where $U(r_i)$ is the energy of a pair of atoms at a distance r_i. To this energy we have to add the interaction energy with the knocked-on atom A_1, which is

$$U_2 = U(OA_1) = U(a_i) .\qquad (A2)$$

These two interaction energies have to be corrected, since a shock between atoms cannot be regarded as a hard-core collision. In fact, Lehmann and Leibfried[20] have shown that the collision is already taking place when the atom A_0 has only arrived in O' and that A_1 is at the same time being pushed away towards A_1' by the same distance $(O'O) = \frac{1}{2}\Delta$. [Here, $\Delta = (2/b)\ln 2$ and is only dependent on the choice of the potential constant b, i.e., the

TABLE V. Threshold energies in various directions for cobalt, zinc, and cadmium crystals.

Direction	Threshold energies/eV		
	cobalt	zinc	cadmium
[0001]	40 ± 3	19^{+2}_{-1}	40
[10$\bar{1}$4]	23 ± 2	25 ± 2	35
[10$\bar{1}$2]	22 ± 1	30 ± 5	35
[10$\bar{1}$1]	40 ± 5	20 ± 2	19 ± 1
[11$\bar{2}$0]	27 ± 2	14^{+2}_{-1}	21^{+2}_{-1}
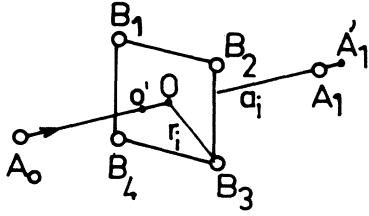
FIG. 10. Last sequence of a passage across a lens.

FIG. 11. Penultimate sequence of a passage across a lens.

hardness of the potential.) Thus, we write instead

$$U_2' = U(O'A_1') . \tag{A3}$$

Moreover, the atom A_0 transmits kinetic energy to the atoms B_i and to A_1 *in the direction of its motion*:

$$E_{kin}' \approx (U_1 + U_2')/(n + 2) , \tag{A4}$$

the mass ratio being $1/(n + 2)$. The kinetic energy transmitted to the atoms B_i perpendicularly to the direction of motion of A_0 need not be taken into account, since it is compensated by a diminution of the potential energy in the lens center due to the repulsive action there of A_0 and the resulting increase of r_i. Thus, the total energy needed for the passage across a lens to give an interstitial is

$$T_d' = U_1 + U_2' + E_{kin}' . \tag{A5}$$

The various r_i and a_i can be found in Table I.

B. Penultimate Sequence

During this collision, the atom A_0 has to transmit to the atom A_1 at least the energy calculated in the preceding section, i.e., T_d'. An atom possessing such an energy can be described by a hard-core radius r_{hc} through the expression $U(r_{hc}) = \frac{1}{2}T_d'$, since only half of the available kinetic energy can be transformed in potential energy in the case of equal masses. Again, due to the correction of Lehmann and Leibfried,[20] the position of A_0 during the collision will be $(OA_0') = a_i - \Delta - r_{hc}$. This means that the atom A_0 has recovered some of its energy lost on the way to O (cf. Fig. 11); the actually required energy is

$$U_3 = n U(A_0' B_i). \tag{A6}$$

This time, we have to add the kinetic energy communicated to B_i perpendicularly to the direction of motion of A_0, since the replusion of B_i will contribute to a decrease of the lens potential and through that to a decrease of U_3. This is a corrective term which amounts to only ~1% of the final threshold. To estimate it, we assume that the momentum received by an atom B_i is $\Delta p \approx f \Delta t$,

where f is the interaction force derived from the potential U and Δt is the time needed to move the atom along a distance $2(OA_0')$ (in front of and behind the lens center); with $U(r) = Ae^{-br}$, we have

$$f = \frac{-dU}{dr} = b U(r_i) \equiv b U_i$$

and

$$E_{kin}^i = \Delta p_i^2/2M = b^2 U_i^2 [2(OA_0')/v]^2/2M$$

$$= b^2 U_i^2 (OA_0')^2/E ,$$

where M and v are the atom mass and velocity and $E = T_d' + U_3$. For n atoms B_i, we obtain as an upper limit:

$$E_{kin}'' = n b^2 U_i^2 (OA_0')^2/T_d' + U_3) . \tag{A7}$$

After subtraction of the zero-point energy, which is the interaction energy of a lattice atom with its 12 neighbors liberated by the creation of a vacancy during the first collision (and neglecting the subsequent contraction around the vacant site) $E_0 = 12 U(a)$, we obtain finally:

$$T_d = T_d' + U_3 + E_{kin}'' - E_0 . \tag{A8}$$

C. Focusing-Collision Sequence

During the propagation of a focusing chain (Fig. 12), the atom A_0 has to be brought to traverse the saddle point O, i.e., to pass from the configuration (O) to configuration (1); this "compression wave" continues to proceed without losing energy, except to the surrounding atoms B_i. The lens in
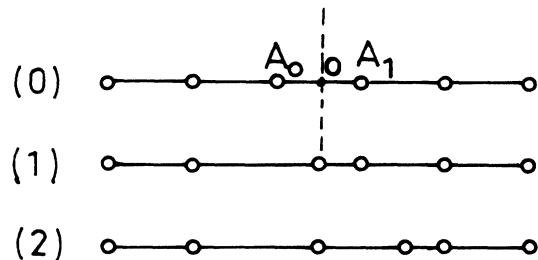
FIG. 12. Propagation of an atom in a focusing collision sequence.

this case is unsymmetric and the potential energy is $U_1^m = 2U(r_i') + 2U(r_i'')$ or, after m collisions:

$$U_1 = m U_1^m . \tag{A9}$$

The compression energy can be expressed as

$$E_{comp} = 2U(\tfrac{1}{2}a + \Delta) - E_0 , \tag{A10}$$

with the usual designations for Δ and E_0. Thus, the total energy spent in a focusing chain is

$$T_d = E_{comp} + U_1 . \tag{A11}$$

The computation of all the thresholds under discussion has been programmed and the details can be found in Ref. 10.

---

[1] J. B. Gibson, A. N. Goland, M. Milgram, and G. H. Vineyard, Phys. Rev. 120, 1229 (1960).

[2] C. Erginsoy, G. H. Vineyard, and A. Englert-Chwoles, Phys. Rev. 133, A595 (1964).

[3] R. v. Jan and A. Seeger, Phys. Status Solidi 3, 465 (1963).

[4] A. Bourret, Phys. Status Solidi A 4, 813 (1971).

[5] P. Jung and W. Schilling, Phys. Rev. B 5, 2046 (1972).

[6] T. Iwata and T. Nihira, J. Phys. Soc. Jap. 31, 1761 (1971).

[7] J. N. Lomer and M. Pepper, Philos. Mag. 16, 1119 (1967).

[8] F. Maury, P. Vajda, A. Lucasson, and P. Lucasson, preceding paper, Phys. Rev. B 8, 5496 (1973).

[9] W. A. McKinley and H. Feshbach, Phys. Rev. 74, 1759 (1948).

[10] F. Maury, thesis (University of Paris at Orsay, 1973) (unpublished).

[11] L. M. Howe, Philos. Mag. 22, 965 (1970).

[12] F. Maury, A. Lucasson, and P. Lucasson, Radiat. Eff. be published).

[13] P. G. Lucasson and R. M. Walker, Phys. Rev. 127, 1130 (1962).

[14] F. Maury, A. Lucasson, and P. Lucasson, Cryst. Lattice Defects 2, 47 (1971).

[15] F. Maury, P. Vajda, A. Lucasson, and P. Lucasson, Radiat. Eff. 10, 239 (1971).

[16] A. A. Abrahamson, Phys. Rev. 178, 76 (1969).

[17] H. H. Andersen and P. Sigmund, Risö Report No. 103, 1965 (unpublished).

[18] P. Lucasson and A. Lucasson, J. Phys. (Paris) 24, 503 (1963).

[19] R. R. Coltman, C. E. Klabunde, J. K. Redman, and A. L. Southern, Radiat. Eff. 7, 235 (1971).

[20] C. Lehmann and G. Liebfried, Z. Phys. 162, 203 (1961).